Investigation of Doping Effect on Structural, Optical, Antibacterial, and Toxicity Properties of Iron Doped Copper Oxide Nanostructures Prepared by Co-Precipitation Route

Anwar, Hafeez*[+]; Abbas, Beenish; Mustafa, Ammara
Department of Physics, University of Agriculture, Faisalabad, 38040, PAKISTAN

Anjum, Fozia
Department of chemistry, Government College University, Faisalabad, PAKISTAN

Ahmad, Fayyaz; Naz, Ishrat
Department of Physics, Riphah International University, Faisalabad, 38000, PAKISTAN

ABSTRACT: *In this work, pure copper oxide and Fe-doped copper oxide nanostructures [$Cu_{1-x}Fe_xO$ where $0 \leq x \leq 0.08$ in steps of 0.02] were synthesized using the co-precipitation method. Iron nitrate nano-hydrate and copper nitrate trihydrate were used as precursors and NaOH was used as precipitating agent. The samples were investigated by X-Ray Diffraction (XRD), Scanning Electron Microscopy (SEM), Energy-Dispersive X-ray Spectroscopy (EDS), and UV-Visible spectroscopy for their structural, morphological, and optical properties, respectively. The effect of iron concentration on antibacterial activity and hemolysis was also investigated for Escherichia coli and Bacillus Subtilis. The XRD pattern showed a single-phase monoclinic structure of CuO nanoparticles. The average crystallite size of pure copper oxide was found 39 nm whereas the average crystallite size of Fe-doped CuO was found in the range 39-44 nm. It was observed that average crystallite size was increased with an increasing iron concentration in CuO. Scanning electron microscopy analysis showed spherical-like morphology and EDS confirmed the presence of iron and copper with proper composition. UV-Vis spectroscopy results showed that the band gap was decreased with increasing iron concentration. Samples prepared with higher concentrations of iron exhibited high E. coli and B. subtilis antibacterial activity. Low hemolytic is safer to be used in various applications such as drug delivery.*

KEYWORDS: *Fe-doped CuO; Co-Precipitation; Structural properties; Antibacterial activity; Hemolysis.*

***** *To whom correspondence should be addressed.*
+ *E-mail*: *hafeez.anwar@gmail.com*
1021-9986/2022/3/777-786 *10/$/6.00*

INTRODUCTION

Transition metals oxides have been attracted due to their physical properties and technological applications such as gas sensors [1], spintronic devices [2], magnetic storage media [3], solar energy conversion [4], electronics [5-6], and catalysis [7-8]. Cupric oxide (CuO) is a key-note p-type semiconductor that has a narrow band gap. The chemical and physical properties of the CuO nanoparticles are strongly dependent on their shape, size, and structure [9]. In the past, nanoparticles were used for different applications and doping of metal oxides was done to enhance their properties in order to employ these in different fields such as solar cells [10], photocatalysis [11], photodegradation [12], and sensors [13]. There are different approaches have been adopted to prepare pure and doped nanoparticles such as thermal decomposition [14], hydrothermal [15], sol-gel [16], and combustion methods. The co-precipitation method has many advantages such as low cost, simplicity, and low process temperature. Nanotechnology has many applications in different fields such as nanomedicine [17], biomedical [18], and drug delivery [19]. Metal oxides such as ZnO, TiO_2, CuO, etc [20-24] and their composites [25-29] have been used extensively as antibacterial agents. As copper oxide and iron oxide are studied individually in terms of their antibacterial activity, it will be interesting to study the antibacterial properties of iron-doped copper oxide [30-33]. A comprehensive study of the already published reports has highlighted the fact that only the effect of iron doping in copper oxide on antibacterial properties has been investigated for various gram-positive and gram-negative bacteria [34-35]. In addition to understanding the role of doping, no sort of work has been done so far to investigate the structure-property relationship of Fe-doped copper oxide. It is considered that any change in size, shape, and structure may affect the Physico-chemical as well as biological properties of the materials. In this research work, we report the structural, morphological, and optical properties of the undoped and doped CuO nanoparticles synthesized by the Co-precipitation method. The prepared samples were analyzed by X-ray diffraction, Scanning electron microscopy, energy-dispersive X-ray spectroscopy, and UV-Vis spectroscopy. Furthermore, the cytotoxic and antibacterial activity of these samples against *E. Coli* and *B. Subtilis* was also investigated from the perspective of the doping and structure-property relationship of these samples. It is expected that there will be an enhancement in antibacterial activity for this doping against different bacteria.

EXPERIMENTAL SECTION

Chemical and reagents

In this work, Copper nitrate [Cu $(NO_3)_2.3H_2O$], and iron nitrate [Fe $(NO_3)_3.9H_2O$] and sodium hydroxide (NaOH) were used. All the chemicals were of analytical grade and used without any further purification. Said compounds were purchased from Sigma-Aldrich.

Synthesis of Fe-doped copper oxide

The schematic diagram of the preparation of Fe-doped CuO nanoparticles [$Cu_{1-x}Fe_xO$ where $0 \leq x \leq 0.08$ in steps of 0.02] is shown in Fig. 1. Stoichiometric amounts of salts such as copper nitrate, iron nitrate, and sodium hydroxide were dissolved in 20 mL of de-ionized water and stirred for 2 h. The precipitates were collected by filtration and washed 2-3 times with de-ionized water to remove by-products such as $NaNO_3$. It was then dried at 80 ºC for 3 h in an oven (Model Shel-Lab) and ground with an agate pestle and mortar to get the fine powder of the prepared sample. The resulting powders were then calcined in air at 800 ºC for 5 h in a furnace (Model SNOL-LHM).

Characterization

The powder X-ray diffraction was performed through XRD system Model (PANalytical) with Nickel filtered CuK_α ($\lambda = 1.5405$ Å) radiation. The average crystallite size was calculated by using Scherer's formula. The scanning electron microscopy (SEM) studies were carried out using SEM Model (JEOL-JSM 5910). The absorption spectra of prepared samples were recorded with UV-Vis spectrophotometer PG Model T-80. The spectra were recorded in the range of 200-800 nm. The average crystallite size, lattice parameters, volume of the unit cell, and theoretical density were calculated by using the following relations

$$D = \frac{0.9\lambda}{B\cos\theta} \quad (1)$$

$$\frac{1}{d^2} = \frac{1}{\sin^2\beta}\left(\frac{h^2}{a^2} + \frac{k^2\sin^2\beta}{b^2} + \frac{l^2}{c^2} - \frac{2hl\cos\beta}{ac}\right) \quad (2)$$

$$V_{cell} = abc\sin\beta \quad (3)$$

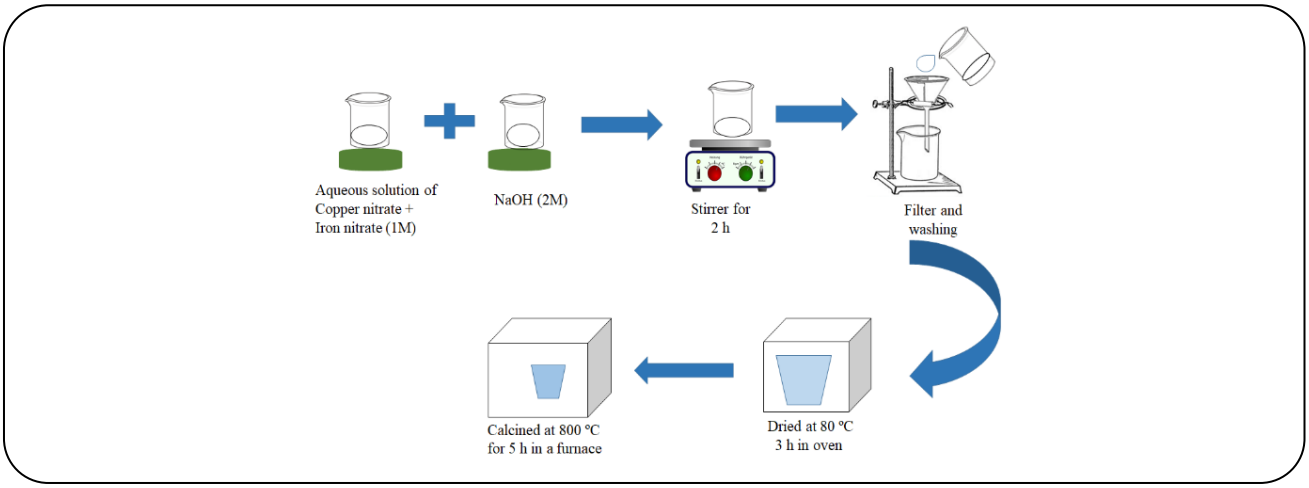

Fig. 1: Preparation of Fe-doped CuO nanoparticles.

$$\text{Density} = \frac{n\,M}{N_A V_{cell}} \quad (4)$$

Where D is average crystallite size, B is line width (FWHM), θ is the angle of diffraction and λ is the wavelength of X-rays used. n is the number of atoms per unit cell, M is the molar weight of the copper oxide, N_A is Avogadro's number and V_{cell} is the volume of the unit cell.

Antibacterial activity evaluation

Selection of bacterial and culture preparation

Escherichia coli, *Bacillus subtil*, Tiron-X, and PBS were used for antibacterial activity. This was done by the good diffusion method. Fresh cultures were prepared using growth media (Nutrient ager, Oxoid UK) for bacterial strains. Sterilized conditions were maintained in order to avoid contamination.

Antimicrobial assay by well diffusion method

Antibacterial activities of pure and Fe-doped CuO nanoparticles were determined by using the good diffusion method [36]. The antimicrobial activity of Fe-doped copper oxide with different concentrations was tested against the bacterial strain. Fresh growth media for the bacterial strain was prepared. In order to minimize the chance of contamination, wet sterilization method was used in which agar solution was first autoclaved at 120 ºC for 20 min. An amount (50 mL) of autoclaved Nutrient agar was taken in Petri plates. To this, 20 µL of the fresh culture of each microorganism was added and mixed well. After the solution solidified, 100 µL of positive control Tiron-X was used as an antibacterial. Then, these Petri plates were incubated at 37 ºC for 24 h. Clear zones were observed for the samples having antibacterial activity in terms of bacterial growth inhibition.

Cytotoxic activity

The cytotoxic activity was determined by the previously reported method [37]. Briefly, 5 mL of the blood of a healthy volunteer was collected in the heparinized tube. Blood was centrifuged at 1500 rpm for 5 min. Plasma was discarded and phosphate buffer saline (PBS) was used for washing the pellet. Prepared sample dispersion (0.5 mL) was mixed in cell suspension of 0.5 mL and this mixture was centrifuged for 5 min. The free hemoglobin in the supernatant was measured in a microplate reader (BioTek, USA) at 540 nm. PBS was used as negative control and Triton-X-100 as a positive control for this assay. The level of percentage hemolysis by the samples was calculated according to the following formula:

$$\%\,\text{Cytotoxic} = \frac{\text{Sample abs} - \text{Negative control abs}}{\text{Postitive control abs}} \times 100 \quad (5)$$

RESULTS AND DISCUSSION

XRD Analysis

The XRD patterns of prepared Fe-doped CuO nanoparticles at different concentrations (0.00, 0.02, 0.04, 0.06 and 0.08) are shown in Fig. 2. X-ray diffraction patterns confirm the crystalline structure of Fe-doped CuO nanoparticles. The observed diffraction peaks at 2θ

Table 1: Structural parameters of prepared pure and Fe-doped CuO nanoparticles from XRD.

Sr. No	Sample concentration %	Average crystallite size (nm)	Lattice constants (Å)			Volume of unit cell (Å)^3	Theoretical density (g/cm^3)
			a	b	c		
1	0.00	43	4.50	3.42	5.05	6.9	7.61
2	0.02	39	4.59	3.42	5.05	7.01	7.52
3	0.04	41	4.14	3.42	5.04	7.04	7.49
4	0.06	42	4.00	3.41	5.15	7.03	7.47
5	0.08	44	4.05	3.42	5.04	6.9	7.60

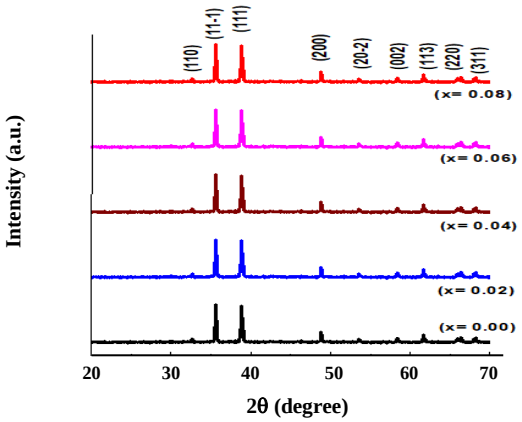

Fig. 2: XRD pattern of Pure and Fe-doped CuO prepared at different concentrations.

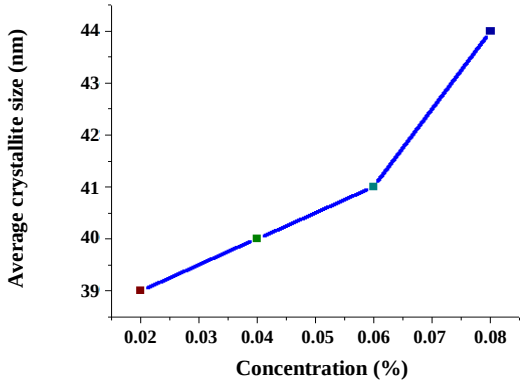

Fig. 3: The variation of crystallite size with different concentrations of iron in CuO.

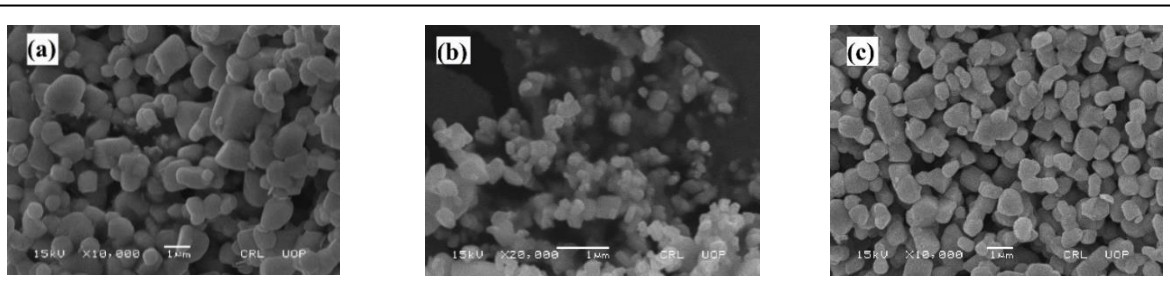

Fig. 4: SEM images of Fe-doped CuO nanoparticles (a) x = 0.00 (b) x = 0.02 (c) x = 0.04.

of 32.63º, 35.63º, 38.83º, 48.83º, 53.57º, 58.38º, 61.61º, 68.14º and 69.43º referred to hkl planes (110), (11$\bar{1}$), (111), (200), (20$\bar{2}$), (002), (113), (220) and (311) respectively. The JCPDS file No. 36-1451 revealed that the synthesized Fe-doped CuO has a monoclinic structure. The average crystallite size, lattice constants, unit cell volume, and theoretical density were calculated from X-ray diffraction data and obtained results are listed in Table 1. It is found that with increasing concentration of Fe in CuO, average crystallite size also increases as shown in Fig. 3 and which is in good accordance with the previously reported work [38].

SEM Analysis

The electron Scanning Electron Microscopy (SEM) images of samples with different concentrations (0.00, 0.02, 0.04) are shown in Fig. 4. Scanning microscopy also revealed the information about surface shape and composition of nanostructure. SEM images show that Fe-doped CuO nanostructures were sphere-like shape at higher concentration and it is evident that at the different concentrations, size and shape have significant effect on the morphology of nanostructures. Particle size from SEM micrographs was analyzed by Image J software. Particle

Table 2: Analyzed parameters of SEM images at 0.00, 0.02 and 0.04 of Fe concentration in CuO.

Sample (x)	Average particle size (nm)	Standard deviation (nm) w/2	Polydispersity (%)	Average grain size (nm)
0.00	294.94	147.47	50	235.60
0.02	162.65	81.65	50	203.05
0.04	237.34	118.67	50	285.31

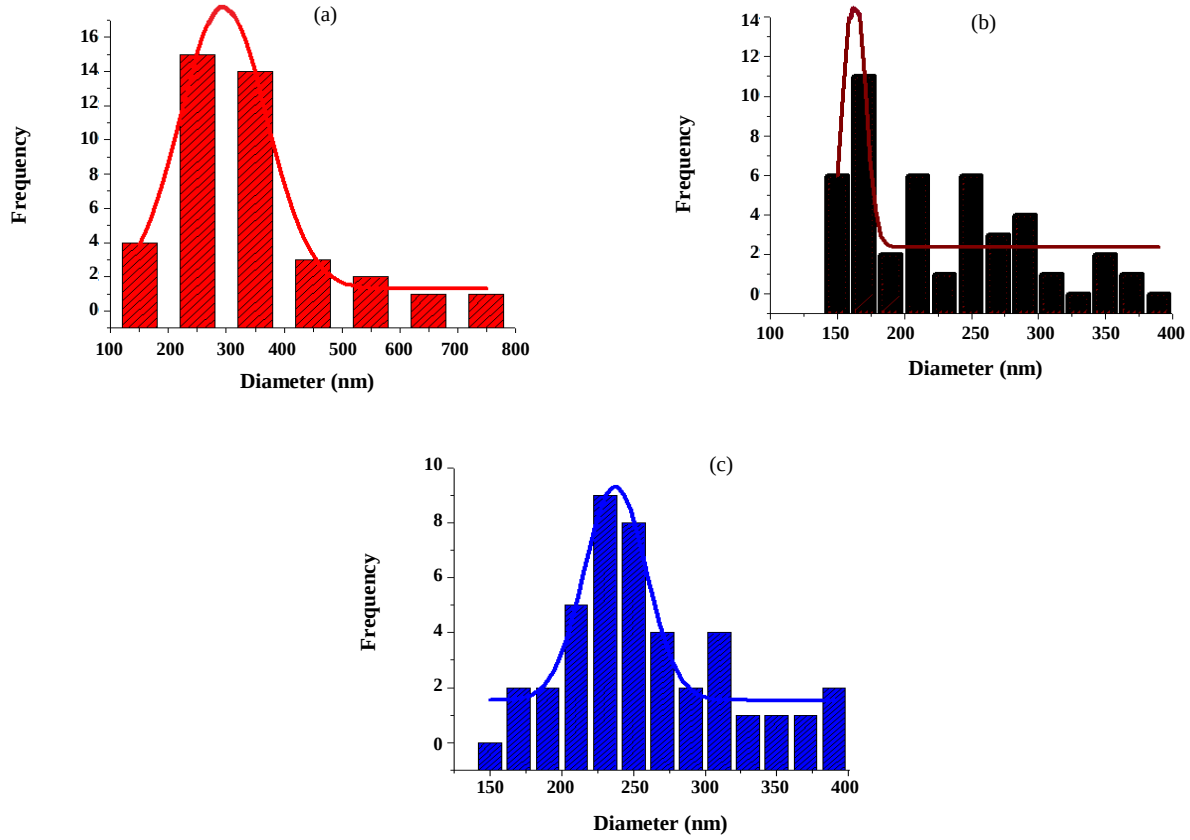

Fig. 5: The particle size distribution of Fe-doped CuO nanoparticles (a) x = 0.00 (b) x = 0.02 (c) x = 0.04.

distribution and related parameters were calculated and shown in Fig. 5 and Table 2.

EDS analysis

Chemical composition analysis of synthesized Fe-doped CuO particles (Cu_{1-x} Fe_xO) at x = 0.02 was carried out and EDS spectrum is shown in Fig. 6. It is evident that the presence of iron which was confirmed in copper oxide and it is also observed that the sample is free from impurities. The analysis shows that the iron composition of 2% is found in close agreement with the used concentration at the time of its synthesis.

UV-Vis analysis

The absorption spectrum of pure copper oxide nanoparticles is shown in Fig. 7(a). The optical band gap was calculated using Tauc's plot in which the following equation [39] was used.

$$\alpha = A\,(E - E_g)^n \qquad (6)$$

Where α is the absorption coefficient having units in cm^{-1}, A is a constant that depends on the nature of the material, E is the photon energy, Eg is the band gap and n is a constant whose values depend upon the nature of electronic transitions. Generally, it has the value of

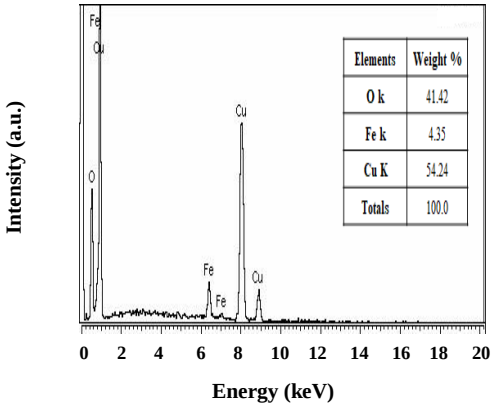

Fig. 6: EDX analysis of Fe-doped copper oxide showing the elemental composition [x = 0.02].

n = ½ for direct transition whereas for indirect it can have a value of n = 2. Figs. 7(b) and 7(c) show tauc's plot for both of these transitions. The indirect and direct band gaps of pure CuO nanoparticles are found to be 1.8 eV and 1.9 eV respectively. Furthermore, band gaps found from these transitions can be used to predict the crystallinity of materials. A higher band gap from direct transition as compared to indirect transition is an indication of crystalline material. Therefore, the prepared pure CuO nanoparticles, in our case, are of crystalline nature and this result also supports the XRD results discussed in previous sections [40].

The absorption spectra of Fe-doped CuO nanoparticles synthesized by the co-precipitation method at different concentrations [0.00, 0.02, and 0.04] are shown in Fig. 8(a). The optical absorption measurements of Fe-doped CuO nanoparticles are carried out in the range of wavelength 200 nm to 800 nm. The absorption of the incident radiation depends on the shape and size of the nanoparticles. The band gaps of the Fe-doped CuO nanoparticles are obtained from the plot between hν vs $(\alpha h\nu)^2$, see Fig. 8(b). The results revealed that the band gap decreased with an increase in iron concentration which showed red shifting. This red shifting in optical band gaps could be due to the quantum confinement effects [41].

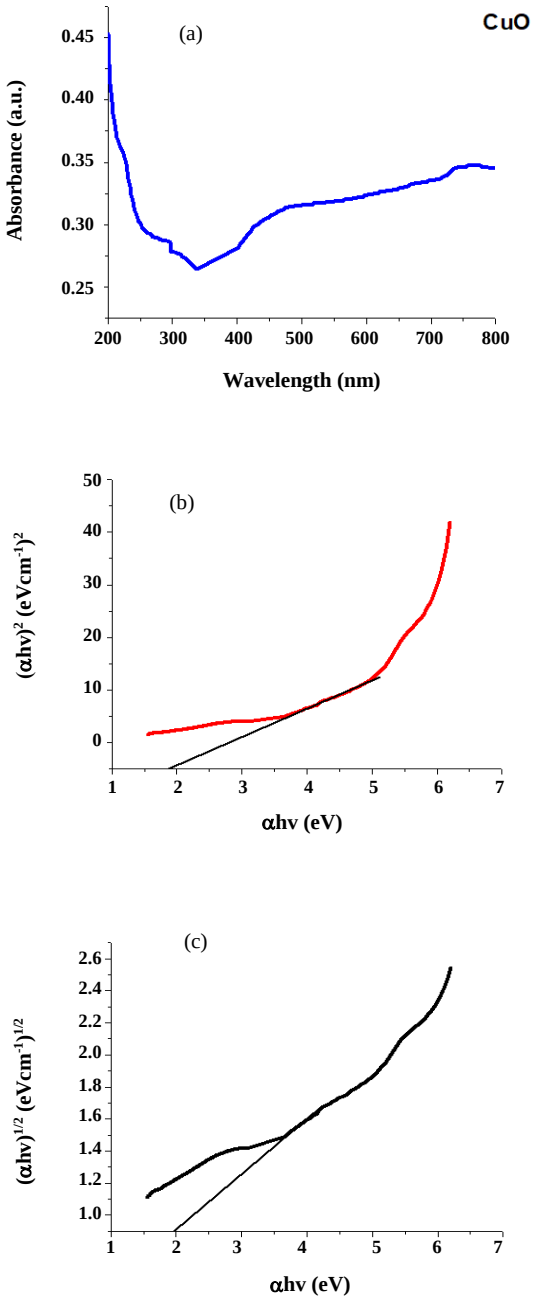

Fig. 7: (a) UV-spectrum of pure copper oxide, Tauc plots of pure CuO (b) direct transitions (c) indirect transitions.

Antibacterial activity

Antimicrobial activity of pure and Fe-doped copper oxide with different concentrations of Fe (0.00, 0.02, 0.04, 0.06, and 0.08) is carried out against *Bacillus subtilis* (Gram-positive) and *Escherichia coli* (Gram-negative) bacterial strains. The Fe-doped copper oxide nanoparticles showed excellent antibacterial results against the selected bacteria. At higher concentrations of iron, the zone of inhibition is increased for *E. coli* and *B. subtilis* as shown in Fig. 9 and Table 2.

Hemolysis activity

This rapid assay is used to screen the cytotoxicity of different samples. The percentage of hemolysis for Fe

Table. 2: Zone of inhibition of Fe-doped CuO at different concentrations against the E. coli and B. subtilis bacterial strain.

Sample	*E. coli* (mm)	*B. subtilis* (mm)
Fe-doped CuO (0.00)	20	11
Fe-doped CuO (0.02)	21	13
Fe-doped CuO (0.04)	24	14
Fe-doped CuO (0.06)	25	16
Fe-doped CuO (0.08)	27	17
Ampicillin	31	19

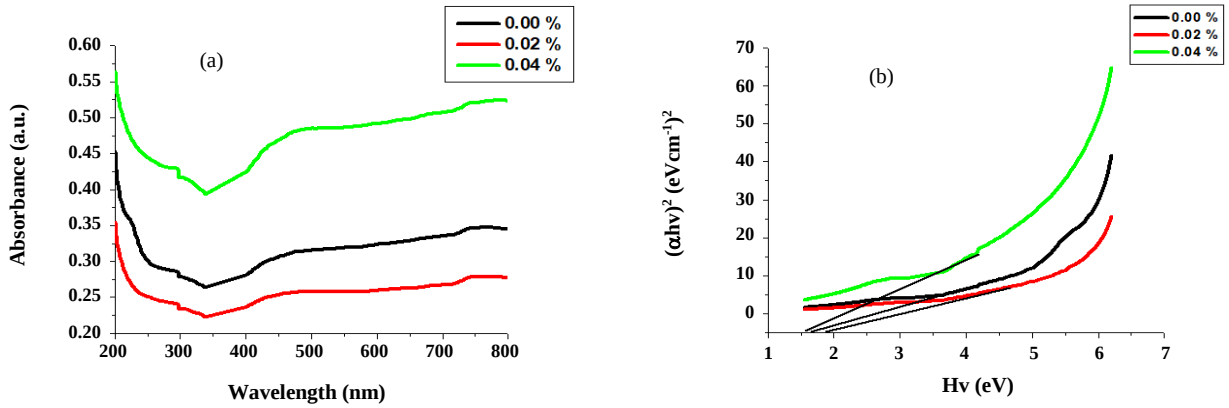

Fig. 8: (a)UV-vis spectrum of different concentrations (0.00, 0.02, 0.04) of Fe doped CuO (b) plot $(\alpha hv)^2$ vs hv.

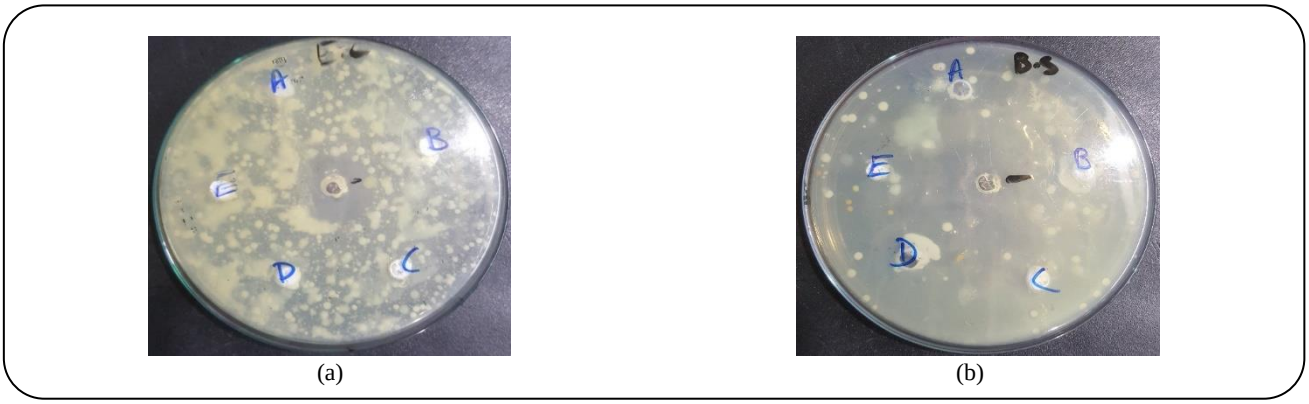

Fig. 9: Zone of inhibition of Fe-doped CuO nanoparticles at different concentrations against (a) E. coli (a) and (b) B. subtilis.

concentrations of 0.00, 0.02, 0.04, 0.06, and 0.08 are shown in Fig. 10. The hemolysis activity is found to be 15. 65 % for pure CuO and for the higher concentration of Fe (0.08 %) in CuO is also found at about 7.95 %. The results show that with an increasing concentration of Fe, hemolysis activity decreases. As a positive control, Triton-X was used and its percentage of hemolysis is 92 %. And negative control PBS was used and its percentage of hemolysis is 1. 12%.

CONCLUSIONS

Fe-doped copper oxide nanoparticles were prepared successfully by co-precipitation method at different concentrations of Fe in CuO nanoparticles and investigated by various techniques such as XRD, SEM, EDS, and UV-Visible spectroscopy. Their antibacterial and hemolytic properties were also investigated. The prepared Fe-doped copper oxide nanoparticles were confirmed with a pure monoclinic phase. The average crystallite size was found

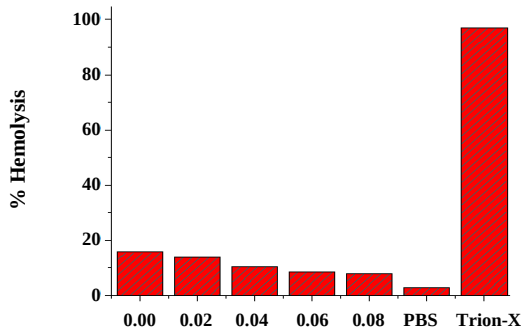

Fig. 10: Hemolysis analysis of Fe-doped copper oxide nanoparticles at different Fe concentrations.

in the range of 39-44 nm. The morphology of the Fe-doped copper oxide was found to be sphere-like. The UV-visible spectroscopy confirmed that the band gap decreased with increased iron concentration from 1.8 eV to1.6 eV. The Fe-doped copper oxide showed promising antibacterial activity against *E. coli* and *B. subtilis* as the zone of inhibition was increased for high iron concentration. It is also found that for higher iron concentration in CuO, the hemolysis activity was low (~ 50 %) as compared to pure CuO. Low hemolytic activity is safer to be used in various applications such as drug delivery.

Acknowledgment

Hafeez Anwar acknowledges the financial assistance provided by Pakistan Science Foundation under project No; PSF-NSF/Eng/P-UAF (05).

Received : Sep. 3, 2020 ; Accepted : Feb. 15, 2021

REFERENCE

[1] Salavati-Niasari M., Davar F., Farhadi M., Synthesis and Characterization of Spinel-Type $CuAl_2O_4$ Nanocrystalline by Modified Sol-Gel Method, *J. of Sol-Gel Science and Technology*, **51**: 48-52 (2009).

[2] Candelaria S.L., Shao Y., Zhou W., Li X., Xiao J., Zhang J.G., Wang Y., Liu J., Li J., Cao G., Nanostructured Carbon for Energy Storage and Conversion, *J. Nano Energy*, **1**: 195-220 (2012).

[3] Xu Y., Chen D., Jiao X., Fabrication of CuO Pricky Microspheres with Tunable Size by a Simple Solution Route, *J. of Physical Chem. B*, **109**: 13561-13566 (2005).

[4] Zheng S.F., Hu J.S., Zhong L.S., Song W.G., Wan L.J., Guo Y.G., Introducing Dual Functional CNT Networks Into CuO Nanomicrospheres Toward Superior Electrode Materials for Lithium-Ion Batteries, *J. Chem of Materials*, **20**: 3617-3622 (2008).

[5] Sconza A., Torzo G., Spectroscopic Measurement of the Semiconductor Energy Gap, *American J. of Physics*, **62**: 732-737 (1994).

[6] Gandhi S., Hari Hara Subramani R., Ramakrishnan T., Sivabalan A., Dhanalakshmi V., Gopinathan Nair M.R., Anbarasan R., Ultrasound Assisted one Pot Synthesis of Nano-Sized CuO and Its Nanocomposite with Poly (vinyl alcohol), *J. Mater Sci.*, **45**: 1688-1694 (2010).

[7] Greenwood R., Review of the Measurement of Zeta Potentials in Concentrated Aqueous Suspensions Using Electroacoustics, *J. Adv. in Colloid and Interface Sci.*, **106**: 55-81 (2010).

[8] Prajapati C.S., Sahay P.P., Growth, Structure and Optical Characterization of Al- doped ZnO Nanoparticle Thin Films, *J. Crystal Res. and Tech.*, **46**: 1086-1092 (2011).

[9] Mondal S., Effect of Manganese Incorporation in ZnO Thin Films Prepared by SILAR, *J. Sci. Soc.*, **10**: 139 (2012).

[10] Liang J., Chen D., Yao X., Zhang K., Qu F., Qin L., Li J., Recent Progress and Development in Inorganic Halide Perovskite Quantum Dots for PhotoelectrochemicaL Applications, *J. Small*, **16**: 1903398 (2019).

[11] He H. Y., He Z., Shen Q., Eco-Friendly Synthesis and Characterizations of Single-Wall Carbon Nanotubes/Ag Nanoparticle Hybrids for Environmental Decontamination, *J. Materials Research Express*, **6**: 035002 (2018).

[12] Shen X., Duan L., Li J., Zhang X., Li X., Lü W., Enhanced Performance of Flexible Ultraviolet Photodetectors Based on Carbon Nitride Quantum Dot/ZnO Nanowire Nanocomposites, *J. Materials Research Express*, **6**: 045002 (2019).

[13] Sa R.R., Matos R. A., Silva V. C., da Cruz Caldas J., da Silva Sauthier M. C., dos Santos W.N.L., Júnior A.D.F.S., Determination of Bioactive Phenolics in Herbal Medicines Containing Cynara scolymus, Maytenus ilicifolia Mart ex Reiss and Ptychopetalum Uncinatum by HPLC-DAD, *J. Microchemical*, **135**: 10-15 (2017).

[14] Garbovskiy Y.A., Glushchenko A.V., Liquid Crystalline Colloids of Nanoparticles: Preparation, Properties, and Applications, *J. in Solid State Physics*, **62**: 1-74 (2010).

[15] Hedayati K., Goodarzi M., Ghanbari D., Hydrothermal Synthesis of Fe_3O_4 Nanoparticles and Flame Resistance Magnetic Poly Styrene Nanocomposite, *J. of Nanostructures*, **7**: 32-39 (2017).

[16] Samson K., Żelazny A., Grabowski R., Ruggiero-Mikołajczyk M., Śliwa M., Pamin K., Lachowska M., Influence of the Carrier and Composition of Active Phase on Physicochemical and Catalytic Properties of Cuag/Oxide Catalysts for Selective Hydrogenolysis of Glycerol, *J. Research on Chemical Intermediates*, **41**: 9295-9306 (2015).

[17] Garnett E., Yang P., Light Trapping in Silicon Nanowire Solar Cells, *J. Nano Letters*, **10**: 1082-1087 (2010).

[18] Arshad M., Ehtisham-ul-Haque S., Bilal M., Ahmad N., Ahmad A., Abbas M., Nisar J., Khan M.I., Nazir A., Ghaffar A., Iqbal M., Synthesis and Characterization of Zn Doped WO_3 Nanoparticles: Photocatalytic, Antifungal and Antibacterial Activities Evaluation, *J. Materials Research Express*, **7**: 015407 (2020).

[19] Upadhyay S. B., Mishra R. K., Sahay P. P., Structural and Alcohol Response Characteristics of Sn-Doped WO_3 Nanosheets, *J. Sensors and Actuators B: Chemical*, **193**: 19-27 (2014).

[20] Adhikari S., Mandal S., Sarkar D., Kim D.H., Madras G., Kinetics and Mechanism of Dye Adsorption on WO_3 Nanoparticles, *J. Applied Surface Science*, **420**: 472-482 (2017).

[21] Anwar H., Rana B.C., Javed Y., Mustafa G., Ahmad M.R., Jamil Y., Akhtar H., Effect of ZnO on Photocatalytic Degradation of Rh B and Its Inhibition Activity for C. Coli Bacteria, *J. Russian Journal of Applied Chemistry*, **91**: 143-149 (2018).

[22] Jesline A., John N.P., Narayanan P. M., Vani C., Murugan S., Antimicrobial Activity of Zinc and Titanium Dioxide Nanoparticles Against Biofilm-Producing Methicillin-Resistant Staphylococcus Aureus, *J. Applied Nanoscience*, **5**: 157-162 (2015).

[23] Saqib S., Munis M. F. H., Zaman W., Ullah F., Shah S.N., Ayaz A., Bahadur S., Synthesis, Characterization and Use of Iron Oxide Nano Particles for Antibacterial Activity, *J. Microscopy Research and Technique*, **82**: 415-420 (2019).

[24] Abbas A., Abussaud B.A., Al-Baghli N.A., Khraisheh, M., Atieh M. A., Benzene Removal by Iron Oxide Nanoparticles Decorated Carbon Nanotubes, *J. of Nanomaterials*, (2016).

[25] Padervand M., Elahifard M. R., Meidanshahi R.V., Ghasemi S., Haghighi S., Gholami M.R., Investigation of the Antibacterial and Photocatalytic Properties of the Zeolitic Nanosized AgBr/TiO_2 Composites, *J. Materials Science in Semiconductor Processing*, **15**: 73-79 (2012).

[26] Padervand M., Jalilian E., Majdani R., Goshadezehn M., BiOCl/AgCl-BiOI/AgI Quaternary Nanocomposite for the Efficient Photodegradation of Organic Wastewaters and Pathogenic Bacteria under Visible Light, *J. of Water Process Engineering*, **29**: 100789 (2019).

[27] Padervand M., Fasandouz F. M., Beheshti A. [Cu-Ag2] O–C3N4 Nanoframeworks for Efficient Photodegradation of Wastewaters, *J. Progress in Reaction Kinetics and Mechanism*, **44**: 175-186 (2019).

[28] Padervand M., Facile Synthesis of the Novel Ag [1-butyl 3-methyl imidazolium] Br Nanospheres for Efficient Photodisinfection of Wastewaters, *J. Chemical Engineering Communications*, **203**: 1532-1537 (2016).

[29] Padervand M., Asgarpour F., Akbari A., Sis B. E., Lammel G., Hexagonal Core-Shell SiO_2 [–MOYI] cl–] Ag Nanoframeworks for Efficient Photodegradation of the Environmental Pollutants and Pathogenic Bacteria, *J. of Inorganic and Organometallic Polymers and Materials*, **29**: 1314-1323 (2019).

[30] Padervand M., Rhimi B., Wang C. One-Pot Synthesis of Novel Ternary $Fe_3N/Fe_2O_3/C_3N_4$ Photocatalyst for Efficient Removal of Rhodamine B and CO_2 Reduction, *J. of Alloys and Compounds*, **852**: 156955 (2021).

[31] Padervand M., Janatrostami S., Karanji A.K., Gholami M.R., Incredible Antibacterial Activity of Noble Metal Functionalized Magnetic Core–Zeolitic Shell Nanostructures, *J. Materials Science and Engineering C*, **35**: 115-121 (2014).

[32] Santos W.G., Schmitt C.C., Neumann M.G., Polymerization of HEMA Photoinitiated by the Safranine/Diphenylborinate System, *J. of Photochemistry and Photobiology A: Chemistry*, **252**: 124-130 (2013).

[33] Heidarpour H., Padervand M., Soltanieh M., Vossoughi M., Enhanced Decolorization of Rhodamine B Solution Through Simultaneous Photocatalysis and Persulfate Activation over Fe/C_3N_4 Photocatalyst, *Journal Chemical Engineering Research and Design*, **153**: 709-720 (2020).

[34] Arokiyaraj S., Saravanan M., Prakash N.U., Arasu M.V., Vijayakumar B., Vincent S., Enhanced Antibacterial Activity of Iron Oxide Magnetic Nanoparticles Treated with Argemone Mexicana L. Leaf Extract: An in Vitro Study, *J. Materials Research Bulletin*, **48**: 3323-3327 (2013).

[35] Lee C., Kim J.Y., Lee W.I., Nelson K.L., Yoon J., Sedlak D.L., Bactericidal Effect of Zero-Valent Iron Nanoparticles on Escherichia Coli, *J. Environmental Science & Technology*, **42**: 4927-4933 (2008).

[36] Khalid S., Afzal N., Khan J. A., Hussain Z., Qureshi A.S., Anwar H., Jamil, Y., Antioxidant Resveratrol Protects Against Copper Oxide Nanoparticle Toxicity in Vivo, *J. Naunyn-Schmiedeberg's Archives of Pharmacology*, **391**: 1053-1062 (2018).

[37] Kadammattil A.V., Sajankila S.P., Prabhu S., Rao B.N., Rao B.S.S., Systemic Toxicity and Teratogenicity of Copper Oxide Nanoparticles and Copper Sulfate, *J. of Nanoscience and Nanotechnology*, **18**: 2394-2404 (2018).

[38] Studer A.M., Limbach L.K., Van Duc L., Krumeich F., Athanassiou E.K., Gerber L.C., Moch H., Stark W.J., Nanoparticle Cytotoxicity Depends on Intracellular Solubility: Comparison of Stabilized Copper Metal and Degradable Copper Oxide Nanoparticles, *J. Toxicology Letters*, **197**: 169-174 (2010).

[39] Sreeju N., Rufus A., Philip D. Studies on Catalytic Degradation of Organic Pollutants and Anti-Bacterial Property Using Biosynthesized CuO Nanostructures, *J. of Molecular Liquids*, **242**: 690-700 (2017).

[40] Yin S.Y., Yuan S.L., Tian Z.M., Liu L., Wang C.H., Zheng X. F., Huo S. X., Effect of Particle Size on the Exchange Bias of Fe-Doped CuO Nanoparticles, *J. of Applied Physics*, **107**: 043909 (2010).

[41] Swatsitang E., Karaphun A., Phokha S., Hunpratub S., Putjuso T., Magnetic and Optical Properties of $Cu_{1-x}F_{ex}O$ Nanosheets Prepared by the Hydrothermal Method, *J. of Sol-Gel Science and Technology*, **83**: 382-393 (2017).